The exclusive formation of α-metalated products can be attributed to the strong basic polarization of the W–H bond in complexes of the type $WH(CO)_2(NO)(PR_3)_2$ (see also Scheme II).

The reaction rate of $WH(CO)_2(NO)(PMe_3)_2$ with $RC{\equiv}CCO_2R'$ is strongly dependent on the kind of R group; the sequence is $R'O_2C > H \gg Ph \approx Me$. The series roughly follows Hammett's parameter σ_p^+ for phenyl substituents, which, according to Swain and Lupton, contains a large degree of resonance contribution R (R = 0.11, 0, –0.13, and –0.18 for the aforementioned substituents, respectively).[33]

(33) Swain, C. G.; Lupton, E. C. *J. Am. Chem. Soc.* **1968**, *90*, 4328. See also: Hansch, C.; Leo, A.; Taft, R. W. *Chem. Rev.* **1991**, *91*, 165.

Especially the large difference in reaction rate between the acetylenes $HC{\equiv}CCO_2Me$ and $MeC{\equiv}CCO_2Me$, cannot be explained by field effects alone, since these are almost identical for H and Me group. However, steric effects may also play a role, and more research is needed to elucidate the electronic and steric influences for C≡C addition reactions.

Acknowledgment. We thank the Swiss National Science Foundation for financial support.

Supplementary Material Available: For **3c**, **5b**, and **5c**, tables of positional and thermal parameters and complete bond lengths and angles (12 pages); tables of structure factors (56 pages). Ordering information is given on any current masthead page.

Pronounced Effect of Substituents on the Intramolecular Electron-Transfer Rates in Mixed-Valence Biferrocenium Triiodide Complexes

Teng-Yuan Dong,* Chi-Chang Schei, Ming-Yhu Hwang, Ting-Yu Lee, Show-Kei Yeh, and Yuh-Sheng Wen

Institute of Chemistry, Academia Sinica, Nankang, Taipei, Taiwan, ROC

Received May 13, 1991

The factors controlling the rate of intramolecular electron transfer in the solid state have been studied for a series of binuclear mixed-valence 1′,1‴-bis(substituted benzyl)biferrocenium triiodide salts, where the substituents in the benzyl unit are *p*-iodo (**1**), *p*-bromo (**2**), *p*-chloro (**3**), *o*-iodo (**4**), and *o*-bromo (**5**). The X-ray structure of neutral 1′,1‴-bis(*p*-bromobenzyl)biferrocene has been determined at 298 K: $P\bar{1}$, a = 5.853 (4) Å, b = 8.380 (3) Å, c = 14.2295 (18) Å, α = 74.622 (15)°, β = 83.940 (23)°, and γ = 86.69 (4)°; Z = 1, D_{calcd} = 1.758 g cm^{-8}, R_F = 0.036, and R_{wF} = 0.038. The Fe–Fe distance is 5.119 (3) Å. Compound **2** crystallizes in the triclinic space group $P\bar{1}$ with one molecule in a unit cell with dimensions a = 9.5505 (24) Å, b = 10.984 (3) Å, c = 11.248 (5) Å, α = 119.71 (3)°, β = 116.04 (3)°, and γ = 76.946 (22)°. The final discrepancy factors are R_F = 0.052 and R_{wF} = 0.039. A decrease in Fe–Fe distance (5.058 (7) Å) has been observed when 1′,1‴-bis(*p*-bromobenzyl)biferrocene is oxidized. The solid-state structure of **2** is composed of parallel sheets of cations and polyiodide ions which contain zigzag chains of alternate I_3^- and I_2 units. The distance of 3.487 (2) Å between neighboring iodine atoms in I_2 and I_3^- units within a chain indicates a nonnegligible interaction. Compound **4** crystallizes in the triclinic space group $P\bar{1}$ with one molecule in a unit cell with dimensions a = 8.149 (4) Å, b = 9.567 (3) Å, c = 12.491 (4) Å, α = 111.78 (3)°, β = 85.97 (4)°, and γ = 108.39 (3)°. The final discrepancy factors for **4** and R_F = 0.056 and R_{wF} = 0.04. The Fe–Fe distance in **4** is 5.082 (8) Å. As expected, the triiodide anion in **4** is situated differently. In contrast to compound **2**, the I_3^- anion in **4** is perpendicular to the fulvalenide ligand. The features in the variable-temperature (77–300 K) ^{57}Fe Mössbauer spectra of **1** include two doublets, which are expected for a mixed-valence cation localized on the time scale of the Mössbauer technique (electron-transfer rates less than $\sim 10^7$ s^{-1}). The valence-trapped electronic structure is also seen for compound **3**. In the case of **2**, at temperatures below 150 K it shows two doublets in the ^{57}Fe Mössbauer spectra and increasing the temperature causes two doublets to become a single "average-valence" doublet at a temperature of ~200 K. In comparison with compounds **1–3**, a single "average-valence" doublet ($\Delta E_Q \approx 1.1$ mm s^{-1}) is seen even at 77 K for **4** and **5**. Thus, there is a dramatic change in electron-transfer rate as the position of halide substituent in the benzyl unit is changed from the para position to the ortho position. EPR and IR data are also presented for **1–5**.

Introduction

Recently, there has been considerable progress made in understanding the factors which control the rate of intramolecular electron transfer in the solid state for mixed-valence compounds.[1] In the case of binuclear mixed-valence biferrocenium compounds,[2-14] it has been found that the nature of the solid-state environment about a

Scheme I

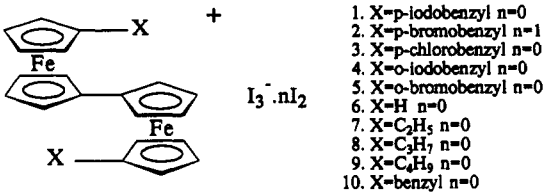

(1) For recent reviews, see: (a) Day, P. *Int. Rev. Phys. Chem.* **1981**, *1*, 149. (b) Brown, D. B., Ed. *Mixed-Valence Compounds, Theory and Applications in Chemistry, Physics, Geology and Biology*; Reidel Publishing Co.: Boston, MA, 1980. (c) Creutz, C. *Prog. Inorg. Chem.* **1983**, *30*, 1–73. (d) Richardson, D. E.; Taube, H. *Coord. Chem. Rev.* **1984**, *60*, 107–129.

0276-7333/92/2311-0573$03.00/0

mixed-valence cation can have a dramatic impact on the rate of intramolecular electron transfer. When there is an onset of dynamics associated with the counterion, or ligands, this will probably influence the rate of intramolecular electron transfer.[2-9]

Compounds 7–10 (Scheme I) give unusual temperature-dependent Mössbauer spectra.[3-6] At temperatures below 200 K they show two doublets, one for the Fe^{II} and the other for the Fe^{III} site. Increasing the sample temperature in each case causes the two doublets to move together with no discernible line broadening and eventually to become a single "average-valence" doublet at temperatures of 275, 245, 275, and 260 K, respectively. Furthermore, pronounced dependency of sample history on the electron-transfer rates has been noted[5] for compounds 6, 9, and 10. X-ray structures have been reported at 298 and 110 K for 8[13] and at 363, 298, and 15 K for 9.[5]

Binuclear mixed-valence complexes 1–5 are of use in understanding how a nearby triiodide can influence the rate of electron transfer. In a previous theoretical paper,[12] we proposed that the cation–anion van der Waals interactions can have a dramatic influence on the rate of electron transfer for a mixed-valence biferrocenium cation. If the suggestion is correct, then relatively minor perturbations of the cation–anion interactions will have pronounced effects on the electronic structure and therefore rate of intramolecular electron transfer. The mixed-valence cation in each of compounds 1–5 serves as a very sensitive probe of the microscopic structure of the structure state. It is of interest to see whether the halide substituent in the benzyl unit, and therefore its instantaneous van der Waals interactions with neighboring triiodide, affects the rate of electron transfer in the mixed-valence cation.

The focus of this paper is the electron transfer in the solid state for the series of mixed-valence biferrocenium salts 1–5. The results of the X-ray structural work for 2,[15] 4, and 1′,1‴-bis(*p*-bromobenzyl)biferrocene, together with the variable-temperature ^{57}Fe Mössbauer, EPR, and IR data, are presented in this paper in an attempt to understand the fundamental nature of electron transfer in mixed-valence biferrocenium compounds.

Experimental Section

Compound Preparation. All manipulations involving air-sensitive materials were carried out by using standard Schlenk techniques under an atmosphere of N_2. Chromatography was performed on neutral alumina oxide (activity II), eluting with hexane–CH_2Cl_2. Dichloromethane was dried over P_2O_5. Samples of biferrocene were prepared according to the literature procedure.[16]

1′,1‴-Bis(substituted benzoyl)biferrocenes. The standard method given below is a modification of the procedure of Yamakawa.[17] The acylating reagent was made up according to the Friedel–Crafts synthesis by mixing 2.5 equimolar equiv of the corresponding benzoyl chloride and excess $AlCl_3$ in dried CH_2Cl_2 at 0 °C under N_2. The excess $AlCl_3$ was filtered off with glass wool.

The acylating reagent was added by means of a dropping funnel over a period of about 1 h to a solution of biferrocene in dried CH_2Cl_2 at 0 °C. The reaction mixture was stirred for 1–3 h at room temperature, and then it was poured into an ice–water mixture. The resulting mixture was separated after the reduction of ferrocenium ion with aqueous $Na_2S_2O_3$. The organic layer was washed with saturated aqueous $NaHCO_3$ and with water, and it was then dried over $MgSO_4$. The solvent was removed under reduced pressure. The red oily residue was chromatographed. The crude product was recrystallized from benzene–hexane. In general, the yields are approximately 40%. The synthesized compounds were identified by NMR (Table I) and mass spectral data.

1′,1‴-Bis(substituted benzyl)biferrocenes. The reduction reaction was carried out by carefully adding, with stirring, small portions of $AlCl_3$ to a mixture of corresponding bis(substituted

Table I. ^1H NMR Data for Neutral Biferrocenes in $CDCl_3$

compd	chem shift[a]
1′,1‴-bis(*p*-chlorobenzyl)-biferrocene	7.10 (d, 4 H), 6.93 (d, 4 H), 4.27 (t, 4 H), 4.12 (t, 4 H), 3.86 (t, 4.1 H), 3.82 (t, 4.1 H), 3.29 (s, 4 H)
1′,1‴-bis(*p*-bromobenzyl)-biferrocene	7.33 (dd, 4 H), 6.91 (dd, 4 H), 4.27 (t, 4 H), 4.15 (t, 4 H), 3.92 (t, 4 H), 3.85 (t, 4 H), 3.32 (s, 4 H)
1′,1‴-bis(*p*-iodobenzyl)-biferrocene	7.50 (dd, 4 H), 6.79 (dd, 4 H), 4.27 (t, 3.8 H), 4.15 (t, 3.8 H), 3.91 (t, 3.8 H), 3.84 (t, 3.8 H), 3.31 (s, 3.7 H)
1′,1‴-bis(*o*-bromobenzyl)-biferrocene	7.44 (dd, 2 H), 7.11 (td, 2 H), 6.98 (m, 2 H), 6.96 (m, 2 H), 4.35 (t, 4.1 H), 4.20 (t, 4.1 H), 3.95 (s, 8 H), 3.50 (s, 4.1 H)
1′,1‴-bis(*o*-iodobenzyl)-biferrocene	7.68 (dd, 2 H), 7.08 (td, 2 H), 6.87 (dd, 2 H), 6.74 (td, 2 H), 4.32 (t, 4 H), 4.15 (t, 4 H), 3.91 (s, 8 H), 3.42 (s, 4 H)
1′,1‴-bis(*p*-bromobenzoyl)-biferrocene	7.62 (d, 4 H), 7.51 (d, 4 H), 4.62 (t, 4 H), 4.37 (t, 4 H), 4.24 (t, 4 H), 4.18 (t, 4 H)
1′,1‴-bis(*p*-iodobenzoyl)-biferrocene	7.74 (d, 4 H), 7.46 (d, 4 H), 4.62 (t, 3.7 H), 4.37 (t, 3.7 H), 4.23 (t, 3.7 H), 4.18 (t, 3.7 H)
1′,1‴-bis(*o*-bromobenzoyl)-biferrocene	7.61 (dd, 2 H), 7.38 (m, 2 H), 7.31 (m, 2 H), 7.28 (m, 2 H), 4.49 (t, 4 H), 4.39 (t, 4 H), 4.33 (m, 8 H)
1′,1‴-bis(*o*-iodobenzoyl)-biferrocene	7.89 (d, 2 H), 7.36 (m, 4 H), 7.10 (m, 2 H), 4.49 (t, 4 H), 4.42 (t, 4 H), 4.34 (m, 8 H)

[a] Shifts were measured relative to the TMS peak; d = doublet, t = triplet, q = quartet, and m = multiplet.

Table II. Elemental Analyses (%) for 1–5

	calcd		found	
compd	C	H	C	H
1	34.53	2.39	34.35	2.27
2	30.42	2.10	31.17	2.10
3	40.84	2.82	40.43	2.71
4	34.53	2.39	34.99	2.21
5	37.51	2.59	38.15	2.42

(2) Hendrickson, D. N.; Oh, S. M.; Dong, T.-Y.; Moore, M. F. *Comments Inorg. Chem.* **1985**, *4* (6), 329.
(3) Dong, T.-Y.; Cohn, M. J.; Hendrickson, D. N.; Pierpont, C. G. *J. Am. Chem. Soc.* **1985**, *107*, 4777.
(4) Cohn, M. J.; Dong, T.-Y.; Hendrickson, D. N.; Geib, S. J.; Rheingold, A. L. *J. Chem. Soc., Chem. Commun.* **1985**, 1095.
(5) Dong, T.-Y.; Hendrickson, D. N.; Iwai, K.; Cohn, M. J.; Reingold, A. L.; Sano, H.; Motoyama, I.; Nakashima, S. *J. Am. Chem. Soc.* **1985**, *107*, 7996.
(6) Iijima, S.; Saida, R.; Motoyama, I.; Sano, H. *Bull. Chem. Soc. Jpn.* **1981**, *54*, 1375.
(7) Nakashima, S.; Masuda, Y.; Motoyama, I.; Sano, H. *Bull. Chem. Soc. Jpn.* **1987**, *60*, 1673.
(8) Nakashima, S.; Katada, M.; Motoyama, I.; Sano, H. *Bull. Chem. Soc. Jpn.* **1987**, *60*, 2253.
(9) Dong, T.-Y.; Kambara, T.; Hendrickson, D. N. *J. Am. Chem. Soc.* **1986**, *108*, 4423.
(10) Dong, T.-Y.; Kambara, T.; Hendrickson, D. N. *J. Am. Chem. Soc.* **1986**, *108*, 5857.
(11) Sorai, M.; Nishimori, A.; Hendrickson, D. N.; Dong, T.-Y.; Cohn, M. J. *J. Am. Chem. Soc.* **1987**, *109*, 4266.
(12) Kambara, T.; Hendrickson, D. N.; Dong, T.-Y.; Cohn, M. J. *J. Chem. Phys.* **1987**, *86*, 2326.
(13) Konno, M.; Hyodo, S.; Iijima, S. *Bull. Chem. Soc. Jpn.* **1982**, *55*, 2327.
(14) Wong, K. Y.; Schatz, P. N. *Prog. Inorg. Chem.* **1981**, *28*, 369.
(15) Dong, T.-Y.; Hwang, M. Y.; Schei, C. C.; Peng, S. M.; Yeh, S. K. *J. Organomet. Chem.* **1989**, *369*, C33.
(16) Rausch, M. D. *J. Org. Chem.* **1961**, *26*, 1802.
(17) Yamakawa, K.; Hisatome, M.; Sako, Y.; Ichida, S. *J. Organomet. Chem.* **1975**, *93*, 219.

Table III. Experimental and Crystal Data for the X-ray Structures

	11	2	4
formular	$C_{34}H_{28}Br_2Fe_2$	$C_{34}H_{28}Br_2Fe_2I_5$	$C_{34}H_{28}Fe_2I_5$
MW	708.1	1342.62	1182.81
cryst syst	triclinic	triclinic	triclinic
space group	$P\bar{1}$	$P\bar{1}$	$P\bar{1}$
a, Å	5.853 (4)	9.5505 (24)	8.149 (4)
b, Å	8.380 (3)	10.984 (3)	9.567 (3)
c, Å	14.2295 (18)	11.248 (5)	12.491 (4)
α, deg	74.622 (15)	119.71 (3)	111.78 (3)
β, deg	83.940 (23)	116.04 (3)	85.97 (4)
γ, deg	86.69 (4)	76.946 (22)	108.39 (3)
ρ_{calcd}, g cm^{-3}	1.758	2.421	2.292
V, Å^3	668.85	920.74	856.86
Z	1	1	1
μ, mm^{-1}	4.07	7.11	5.33
λ, Å	0.709 30 (Mo K$\bar{\alpha}$)	0.709 30 (Mo K$\bar{\alpha}$)	0.709 30 (Mo K$\bar{\alpha}$)
2θ limits, deg	49.8	49.9	49.8
max, min trans coeff	1.0, 0.661	1.0, 0.802	1.0, 0.628
R_F	0.036	0.052	0.056
R_{wF}	0.038	0.039	0.040

benzoyl)biferrocene and $LiAlH_4$ in dried ether. After 30 min, the solution become yellow, an excess of H_2O was added to it, and the ether layer was separated. The ether layer was washed with H_2O and dried over $MgSO_4$. After the evaporation of the solvent, the crude product was chromatographed and recrystallized from hexane–benzene in a yield of approximately 90%. Table I lists the ^1H NMR data for the synthesized compounds.

Mixed-Valence Compounds 1–5. The triiodide salts were prepared according to the simple procedure previously reported for biferrocenium triiodide. The elemental analyses are given in Table II.

Physical Methods. At the Academia Sinica, ^{57}Fe Mössbauer measurements were made on a constant-acceleration-type instrument. The source, which originally consisted of 35 mCi of ^{57}Co diffused into a 12-μm rhodium matrix, is connected to a Ranger Scientific Model VT-900 velocity transducer. An Ortec Model 5600 multichannel analyzer, scanned over 1024 channels, receives the logic pulses from the single-channel analyzer. Computer fittings of the ^{57}Fe Mössbauer data to Lorentzian lines were carried out with a modified version of a previously reported program.[18] Velocity calibrations were made using a 99.99% pure 10-μm iron foil. Typical line widths for all three pairs of iron lines fell in the range 0.25–0.28 mm s^{-1}. Isomer shifts are reported with respect to iron foil at 300 K.

^1H NMR spectra were run on a Bruker MSL 200 spectrometer. Mass spectra were obtained with a VG250-70S system. Electron paramagnetic resonance data (X-band) were collected with a Bruker ER200D-SRC spectrometer. The magnetic field was calibrated with a Bruker ER035M NMR gauss meter. DPPH was used to gauge the microwave frequency. A direct-immersion dewar, which was inserted into the cavity, was used to obtain 77 K data.

Electrochemical measurements were carried out with a Princeton Applied Research Model 173 instrument. Cyclic voltammetry was performed with a stationary Pt electrode, which was cleaned after each run. Duplicate runs were made on each sample. In most cases the measurements were run on 1×10^{-3} M actonitrile solutions with 0.1 M $(n\text{-}C_4H_9)_4NBF_4$ as the supporting electrolyte. Degassing with nitrogen prefaced each run. The potentials quoted in this work are referred to a saturated aqueous calomel electrode at 25 °C.

Structure Determination of 1′,1‴-Bis(*p*-bromobenzyl)-biferrocene (11). An orange, needlelike crystal (0.15 × 0.25 × 0.80 mm), which was grown by slow evaporation from a hexane solution, was used for data collection at 298 K. Cell dimensions and space group data were obtained by standard methods on an Enraf Nonius CAD4 diffractometer. The θ–2θ scan technique was used to record the intensities for all reflections for which $1° < 2\theta < 49.8°$. Absorption corrections were made with empirical ψ rotation. Of the 2331 independent intensities, there were 2000 with $F_o > 2.5\sigma(F_o^2)$, where $\sigma(F_o^2)$ were estimated from counting statistics. These data were used in the final refinement of the structural parameters. The X-ray crystal data are summarized in Table III.

A three-dimensional Patterson synthesis was used to determine the heavy-atom positions, which phased the data sufficiently well to permit location of the remaining non-hydrogen atoms from Fourier synthesis. All non-hydrogen atoms were refined anisotropically. During the final cycles of refinement fixed hydrogen contributions with C–H bond lengths fixed at 1.08 Å were applied. The final positional parameters for all atoms can be found in Table IV, and the selected bond distances and angles are given in Table V. Listings of the thermal parameters and observed and calculated structure factors are given the supplementary material.

Structure Determination of 2. Blocky, needlelike crystals (0.2 × 0.2 × 0.2 mm), which were grown by slowly diffusing the hexane solution of I_2 into a benzene solution of 1′,1‴-bis(*p*-

Table IV. Atom Coordinates and Thermal Parameters (Å^2) for 11

atom	x	y	z	B_{iso}[a]
Br	0.20990 (7)	0.31498 (4)	0.99827 (2)	3.54 (2)
Fe	−0.52773 (7)	−0.21509 (5)	0.66603 (3)	1.83 (2)
C(1)	−0.5315 (5)	−0.0855 (4)	0.5217 (2)	2.02 (12)
C(2)	−0.3830 (6)	−0.2284 (4)	0.5312 (2)	2.51 (14)
C(3)	−0.5155 (7)	−0.3712 (4)	0.5771 (2)	3.02 (15)
C(4)	−0.7468 (6)	−0.3170 (4)	0.5960 (2)	3.04 (15)
C(5)	−0.7568 (6)	−0.1414 (4)	0.5627 (2)	2.44 (13)
C(6)	−0.4082 (5)	−0.0605 (4)	0.7389 (2)	2.20 (12)
C(7)	−0.2660 (6)	−0.2055 (4)	0.7485 (2)	2.46 (14)
C(8)	−0.4023 (6)	−0.3449 (4)	0.7942 (2)	2.72 (14)
C(9)	−0.6303 (6)	−0.2864 (4)	0.8128 (2)	2.54 (13)
C(10)	−0.6343 (6)	−0.1116 (4)	0.7790 (2)	2.42 (14)
C(11)	−0.3322 (6)	0.1150 (4)	0.6988 (2)	2.78 (14)
C(12)	−0.2063 (6)	0.1737 (4)	0.7705 (2)	2.29 (13)
C(13)	−0.2829 (6)	0.1354 (4)	0.8694 (2)	3.09 (15)
C(14)	−0.1642 (6)	0.1803 (4)	0.9366 (2)	3.15 (15)
C(15)	0.0369 (6)	0.2655 (4)	0.9045 (2)	2.55 (13)
C(16)	0.1144 (6)	0.3111 (4)	0.8069 (2)	2.81 (14)
C(17)	−0.0076 (6)	0.2643 (4)	0.7408 (2)	2.72 (14)
H(2)	−0.21	−0.23	0.51	3.0 (7)
H(3)	−0.45	−0.49	0.60	4.1 (9)
H(4)	−0.88	−0.40	0.64	5.3 (10)
H(5)	−0.91	−0.06	0.57	3.9 (8)
H(7)	−0.10	−0.21	0.72	3.9 (8)
H(8)	−0.36	−0.47	0.81	3.1 (7)
H(9)	−0.77	−0.36	0.85	2.7 (7)
H(10)	−0.77	−0.02	0.78	4.2 (9)
H(11A)	−0.48	0.19	0.68	4.3 (9)
H(11B)	−0.25	0.13	0.63	2.8 (7)
H(13)	−0.43	0.07	0.90	3.4 (8)
H(14)	−0.23	0.15	1.01	3.1 (7)
H(16)	0.26	0.38	0.78	3.5 (8)
H(17)	0.05	0.29	0.67	4.2 (9)

[a] B_{iso} is the mean of the principal axes of the thermal ellipsoid.

(18) Lee, J. F.; Lee, M. D.; Tseng, P. K. *Chemistry* **1987**, *45*, 50.

Table V. Selected Bond Distances (Å) and Bond Angles (deg) for 1′,1‴-Bis(*p*-bromobenzyl)biferrocene (11), 2, and 4

	11	2	4		11	2	4
			Distances				
Fe–C(1)	2.055 (3)	2.074 (6)	2.079 (7)	C(6)–C(10)	1.427 (5)	1.41 (1)	1.43 (1)
Fe–C(2)	2.043 (3)	2.058 (6)	2.058 (8)	C(6)–C(11)	1.505 (4)	1.50 (1)	1.50 (1)
Fe–C(3)	2.041 (3)	2.053 (7)	2.053 (8)	C(7)–C(8)	1.420 (5)	1.41 (1)	1.39 (2)
Fe–C(4)	2.053 (3)	2.046 (7)	2.052 (8)	C(8)–C(9)	1.418 (5)	1.42 (1)	1.40 (2)
Fe–C(5)	2.045 (3)	2.068 (7)	2.057 (8)	C(9)–C(10)	1.415 (5)	1.42 (1)	1.45 (1)
Fe–C(6)	2.053 (3)	2.093 (6)	2.082 (7)	C(11)–C(12)	1.515 (4)	1.52 (1)	1.52 (1)
Fe–C(7)	2.043 (3)	2.058 (7)	2.081 (9)	C(12)–C(13)	1.388 (4)	1.38 (1)	1.42 (1)
Fe–C(8)	2.046 (3)	2.048 (6)	2.044 (9)	C(12)–C(17)	1.392 (5)	1.37 (1)	1.36 (1)
Fe–C(9)	2.048 (3)	2.062 (6)	2.046 (8)	C(13)–C(14)	1.379 (5)	1.39 (1)	1.36 (1)
Fe–C(10)	2.047 (3)	2.067 (6)	2.079 (8)	C(14)–C(15)	1.384 (5)	1.37 (1)	1.37 (1)
C(1)–C(1)[a]	1.455 (6)	1.45 (1)	1.45 (1)	C(15)–C(16)	1.373 (5)	1.39 (1)	1.37 (1)
C(1)–C(2)	1.424 (5)	1.44 (1)	1.43 (1)	C(16)–C(17)	1.386 (5)	1.38 (1)	1.39 (1)
C(1)–C(5)	1.436 (4)	1.43 (1)	1.43 (1)	Br–C(15)	1.899 (3)	1.91 (2)	
C(2)–C(3)	1.430 (5)	1.40 (1)	1.42 (1)	I(3)–C(17)			2.114 (8)
C(3)–C(4)	1.425 (6)	1.43 (1)	1.40 (1)	I(1)–I(2)		2.925 (2)	2.918 (1)
C(4)–C(5)	1.421 (5)	1.42 (1)	1.42 (1)	I(3)–I(3)[a]		2.741 (2)	
C(6)–C(7)	1.417 (5)	1.42 (1)	1.42 (1)				
			Angles				
C(1)–Fe–C(6)	107.36 (12)	110.4 (3)	111.7 (3)	C(1)[a]–C(1)–C(5)	126.1 (3)	125.7 (6)	126.7 (7)
C(1)–Fe–C(7)	123.26 (13)	123.8 (3)	127.4 (3)	C(2)–C(1)–C(5)	107.3 (3)	108.4 (6)	107.9 (6)
C(1)–Fe–C(8)	159.64 (14)	158.1 (3)	161.0 (5)	C(1)–C(2)–C(3)	108.3 (3)	107.4 (6)	107.3 (7)
C(1)–Fe–C(9)	158.31 (13)	160.9 (3)	158.7 (4)	C(2)–C(3)–C(4)	108.1 (3)	108.6 (6)	108.6 (7)
C(1)–Fe–C(10)	122.57 (13)	125.9 (3)	124.2 (3)	C(3)–C(4)–C(5)	107.7 (3)	108.7 (7)	108.9 (7)
C(2)–Fe–C(6)	122.01 (13)	124.6 (3)	124.7 (3)	C(1)–C(5)–C(4)	108.6 (3)	106.9 (6)	107.2 (7)
C(2)–Fe–C(7)	107.43 (13)	107.5 (3)	109.7 (4)	C(7)–C(6)–C(10)	107.2 (3)	107.3 (6)	108.2 (8)
C(2)–Fe–C(8)	123.40 (14)	121.1 (3)	123.2 (4)	C(7)–C(6)–C(11)	126.3 (3)	125.0 (6)	127.5 (8)
C(2)–Fe–C(9)	159.73 (13)	156.5 (3)	157.9 (4)	C(10)–C(6)–C(11)	126.4 (3)	127.7 (6)	124.3 (8)
C(2)–Fe–C(10)	158.21 (13)	161.1 (3)	159.9 (3)	C(6)–C(7)–C(8)	108.5 (3)	108.4 (6)	108.8 (9)
C(3)–Fe–C(6)	158.00 (14)	159.1 (3)	158.6 (4)	C(7)–C(8)–C(9)	107.9 (3)	108.4 (6)	108.8 (9)
C(3)–Fe–C(7)	122.25 (15)	122.6 (3)	122.3 (4)	C(8)–C(9)–C(10)	107.9 (3)	107.0 (6)	108.5 (8)
C(3)–Fe–C(8)	107.34 (13)	106.5 (3)	106.1 (4)	C(6)–C(10)–C(9)	108.5 (3)	108.9 (6)	105.7 (8)
C(3)–Fe–C(9)	123.21 (13)	121.7 (3)	121.2 (3)	C(6)–C(11)–C(12)	112.4 (2)	109.0 (5)	114.8 (6)
C(3)–Fe–C(10)	159.59 (14)	158.4 (3)	158.3 (3)	C(11)–C(12)–C(13)	120.9 (3)	119.5 (6)	121.1 (7)
C(4)–Fe–C(6)	159.94 (14)	159.5 (3)	161.4 (4)	C(11)–C(12)–C(17)	121.6 (3)	121.6 (7)	122.0 (7)
C(4)–Fe–C(7)	158.06 (14)	158.63 (3)	155.6 (4)	C(13)–C(12)–C(17)	117.4 (3)	118.6 (6)	116.9 (7)
C(4)–Fe–C(8)	122.15 (13)	122.7 (3)	120.0 (4)	C(12)–C(13)–C(14)	121.8 (3)	121.1 (7)	120.9 (8)
C(4)–Fe–C(9)	107.45 (13)	107.5 (3)	106.0 (4)	Br–C(15)–C(14)	118.8 (2)	119.3 (6)	
C(4)–Fe–C(10)	123.52 (14)	123.7 (3)	123.5 (4)	Br–C(15)–C(16)	120.0 (3)	118.4 (6)	
C(5)–Fe–C(6)	123.72 (13)	124.7 (3)	126.6 (3)	I(3)–C(17)–C(12)			121.0 (6)
C(5)–Fe–C(7)	159.98 (13)	159.6 (3)	163.2 (3)	I(3)–C(17)–C(16)			116.5 (6)
C(5)–Fe–C(8)	157.93 (13)	159.1 (3)	155.9 (4)	C(14)–C(15)–C(16)	121.1 (3)	122.3 (7)	120.4 (8)
C(5)–Fe–C(9)	122.32 (13)	123.9 (3)	121.6 (4)	C(15)–C(16)–C(17)	118.8 (3)	117.6 (7)	118.8 (8)
C(5)–Fe–C(10)	107.92 (14)	109.7 (3)	108.3 (3)	C(12)–C(17)–C(16)	121.8 (3)	122.1 (7)	122.4 (7)
C(1)[a]–C(1)–C(2)	126.7 (3)	125.5 (6)	125.1 (7)	I(2)–I(1)–I(2)[a]		180.0	180.0

[a] The following atoms have symmetry equivalents: C(1), $-x$, $-y$, $-z$ for 11, $-x$, $2-y$, $1-z$ for 2, and $1-x$, $1-y$, $1-z$ for 4; I(3), $-x$, $1-y$, $1-z$; I(2), $-x$, $-y$, $-z$.

bromobenzyl)biferrocene, were sealed in Lindemann glass capillaries filled with N_2 gas. It was found that when these crystals were exposed to X-rays in air, they suffer some decomposition over a period of time. Data were collected to a 2θ value of 49.9°. The data were also corrected for absorption with an empirical ψ rotation. Of the 3246 independent intensities, there were 2403 with $F_o^2 > 2.5\sigma(F_o^2)$. These data were used in the final refinement of the structural parameters. Details of data collection and unit cell parameters are given in Table III.

Structure refinement was carried out in the same manner as described for 1′,1‴-bis(*p*-bromobenzyl)biferrocene. The greatest residual electron density upon completion of refinement was in the vicinity of the iodide atoms. Atomic coordinates are given in Table VI. The selected bond distances and angles are given in Table V. Listings of the thermal parameters and observed and calculated structure factors are available as supplementary material.

Structure Determination of 4. A blocky crystal (0.5 × 0.16 × 0.01 mm) was obtained following the same procedure as for 2. Of the 3014 independent intensities, there were 2139 with $F_o > 2.5\sigma(F_o^2)$. These data were used in the final refinement of structural parameters. The structure was solved by the heavy-atom method to locate the I positions and successive Fourier maps to reveal the whole molecule and refined with a weighted least-squares routine. The unit cell parameters are given in Table III. Atomic coordinates and the selected bond distances and angles are given in Tables VII and V, respectively. Listings of the observed and calculated structure factors and thermal parameters are available as supplementary material.

Results and Discussion

Single-Crystal X-ray Structure of 1′,1‴-Bis(*p*-bromobenzyl)biferrocene (11). The results of our crystallographic study at 298 K show that it crystallizes in the triclinic space group $P\bar{1}$. The molecule exists in a trans conformation with the two iron ions on opposite sides of the planar fulvalenide ligand. A perspective drawing of the molecule is shown in Figure 1, and selected bond distances and angles are given in Table V. The dihedral angle between the two five-membered rings of each ferrocene moiety is 0.48 (4)°; furthermore, the two rings are nearly eclipsed with an average staggering angle of 1.5 (3)°. The average bond distance (2.047 (3) Å) from the iron atom to the five carbon atoms of the fulvalenide is the same as that from the iron atom to the five carbon atoms of the benzylcyclopentadienyl ring. This distance is closer to the value of 2.045 Å found for ferrocene[19] than to the value

(19) Seiler, P.; Dunitz, J. D. *Acta Crystallogr., Sect. B* **1979**, *35*, 1068.

Table VI. Atomic Coordinates and Thermal Factors (Å²) for 2

atom	x	y	z	B_{iso}[a]
I(1)	0.0	0.0	0.0	3.55 (5)
I(2)	0.28832 (7)	0.09527 (6)	0.26468 (7)	4.92 (4)
I(3)	0.08896 (8)	0.38883 (6)	0.44088 (7)	5.05 (4)
Br	0.69381 (11)	0.29002 (10)	0.09191 (11)	5.46 (6)
Fe	−0.10109 (11)	0.81219 (9)	0.23369 (10)	2.20 (5)
C(1)	−0.0720 (8)	0.9877 (7)	0.4357 (7)	2.6 (4)
C(2)	−0.1037 (9)	1.0272 (7)	0.3220 (8)	3.0 (4)
C(3)	−0.2502 (9)	0.9733 (7)	0.2113 (8)	3.5 (5)
C(4)	−0.3087 (9)	0.8976 (8)	0.2522 (8)	3.6 (5)
C(5)	−0.1992 (8)	0.9054 (7)	0.3908 (8)	3.0 (4)
C(6)	0.1009 (8)	0.6873 (6)	0.2502 (7)	2.4 (4)
C(7)	0.0666 (8)	0.7360 (7)	0.1449 (7)	2.6 (4)
C(8)	−0.0819 (8)	0.6868 (7)	0.0330 (7)	2.8 (4)
C(9)	−0.1426 (8)	0.6084 (7)	0.0684 (7)	2.9 (4)
C(10)	−0.0291 (9)	0.6104 (7)	0.2037 (7)	2.8 (4)
C(11)	0.2518 (9)	0.7089 (8)	0.3806 (8)	3.4 (4)
C(12)	0.3745 (8)	0.6108 (7)	0.3269 (7)	2.8 (4)
C(13)	0.4544 (9)	0.6501 (8)	0.2704 (9)	3.6 (5)
C(14)	0.5497 (9)	0.5557 (8)	0.2039 (9)	3.6 (5)
C(15)	0.5663 (8)	0.4235 (8)	0.1912 (8)	3.4 (4)
C(16)	0.4928 (9)	0.3818 (8)	0.2474 (8)	3.5 (5)
C(17)	0.3972 (9)	0.4786 (8)	0.3149 (8)	3.3 (4)
H(2)	−0.034	1.083	0.321	3.7
H(3)	−0.304	0.985	0.117	4.2
H(4)	−0.413	0.847	0.191	4.2
H(5)	−0.208	0.861	0.447	3.8
H(7)	0.137	0.797	0.150	3.4
H(8)	−0.136	0.704	−0.058	3.5
H(9)	−0.248	0.561	0.010	3.5
H(10)	−0.039	0.564	0.258	3.4
H(11A)	0.285	0.810	0.434	4.0
H(11B)	0.238	0.689	0.454	4.0
H(13)	0.442	0.750	0.286	4.2
H(14)	0.607	0.584	0.163	4.4
H(16)	0.510	0.283	0.239	4.3
H(17)	0.340	0.450	0.356	4.1

[a] B_{iso} is the mean of the principal axes of the thermal ellipsoid.

Table VII. Atomic Coordinates and Thermal Factors (Å²) for 4

atom	x	y	z	B_{iso}[a]
I(1)	0.0 (0)	0.0 (0)	0.0 (0)	3.98 (4)
I(2)	−0.14831 (9)	−0.12782 (7)	0.17657 (5)	4.80 (3)
I(3)	−0.16282 (8)	0.13783 (7)	0.49597 (5)	3.96 (3)
Fe	0.52502 (14)	0.68030 (13)	0.71127 (9)	2.69 (5)
C(1)	0.5674 (9)	0.5649 (8)	0.5394 (6)	2.4 (3)
C(2)	0.5946 (10)	0.7296 (9)	0.5644 (6)	2.9 (4)
C(3)	0.7300 (10)	0.8173 (9)	0.6523 (7)	3.5 (4)
C(4)	0.7828 (10)	0.7111 (10)	0.6826 (7)	3.4 (4)
C(5)	0.6821 (10)	0.5537 (9)	0.6150 (7)	3.1 (4)
C(6)	0.2712 (10)	0.5874 (10)	0.7508 (7)	3.3 (4)
C(7)	0.3104 (12)	0.7519 (11)	0.7765 (8)	4.6 (5)
C(8)	0.4520 (14)	0.8329 (12)	0.8556 (9)	5.8 (6)
C(9)	0.5020 (12)	0.7232 (14)	0.8839 (7)	5.3 (6)
C(10)	0.3897 (11)	0.5656 (11)	0.8182 (7)	3.9 (5)
C(11)	0.1281 (11)	0.4555 (10)	0.6713 (7)	4.0 (4)
C(12)	−0.0384 (10)	0.4051 (10)	0.7291 (7)	3.1 (4)
C(13)	−0.0605 (11)	0.4929 (11)	0.8458 (7)	4.1 (5)
C(14)	−0.2070 (12)	0.4438 (12)	0.8987 (7)	4.5 (5)
C(15)	−0.3384 (12)	0.3099 (12)	0.8394 (8)	4.7 (5)
C(16)	−0.3241 (11)	0.2239 (11)	0.7256 (8)	3.9 (5)
C(17)	−0.1723 (10)	0.2731 (10)	0.6726 (7)	3.1 (4)
H(2)	0.506	0.778	0.538	3.3
H(3)	0.756	0.942	0.703	3.8
H(4)	0.860	0.746	0.758	3.9
H(5)	0.674	0.444	0.632	3.7
H(7)	0.263	0.801	0.725	5.4
H(8)	0.533	0.952	0.880	5.3
H(9)	0.625	0.735	0.928	5.8
H(10)	0.413	0.450	0.801	4.3
H(13)	0.045	0.601	0.895	4.7
H(14)	−0.219	0.512	0.991	5.2
H(15)	−0.459	0.276	0.880	5.4
H(16)	−0.429	0.119	0.678	4.8
H(11A)	0.102	0.506	0.601	3.8
H(11B)	0.159	0.343	0.641	3.8

[a] B_{iso} is the mean of the principal axes of the thermal ellipsoid.

of 2.075 Å found for the ferrocenium cation.[20] The distance between centers of mass (COM) of the two rings is 3.302 (1) Å. The average C–C bond length (1.423 (5) Å) in the rings agrees well with that in ferrocene (1.42 Å).[19] The distance between the two iron atoms is 5.119 (3) Å.

Single-Crystal X-ray Structure of 2. Compound **2** crystallizes at 298 K in the triclinic space group $P\bar{1}$. Figure 2 shows the molecular structures and atomic labeling schemes for the cation (A) and anion (B). A stereoview of the molecule is illustrated in Figure 3. Atomic coordinates and important metrical parameters are given in Tables VI and V, respectively. Compound **2** has the same trans conformation found for the dialkyl analogues.[5,13] A direct comparison was made between neutral 1′,1‴-bis(*p*-bromobenzyl)biferrocene and mixed-valence compound **2** (see Table VIII). Mean bond distances between the iron atom and the five carbon atoms of a given ring are 2.060 (7) and 2.066 (6) Å for the η^5-C_5H_4(fulvalenide) and η^5-C_5H_5 rings, respectively. The average of these two values, i.e., 2.063 Å, is larger than that for neutral 1′,1‴-bis(*p*-bromobenzyl)biferrocene. It also lies midway between the 2.045 Å observed for ferrocene[19] and 2.075 Å observed for the ferrocenium cation.[20] The Fe–Fe distance is decreased from 5.119 (3) Å for the neutral compound to 5.058 (7) Å for **2**. From Table V, there is no significant difference for C–C bond distances in the rings between compound **2** (1.42 (1) Å) and 1′,1‴-bis(*p*-bromobenzyl)biferrocene (1.423 (5) Å). The distance between centers of mass is 3.344 (1) Å. Such an increase in COM–COM distance has been observed when ferrocenes are oxidized to the corresponding ferrocenium ions.[20,21] The plane of the oxidized benzylcyclopentadienyl ligand forms a dihedral angle of 3.3 (4)° with the fulvalenide plane. The two cyclopentadienyl rings in each ferrocene moiety are nearly eclipsed with an average staggering angle of 1.2 (1)°. The site symmetry imposed on the mixed-valence cation obviously requires that both iron centers of the cation are in equivalent positions in the unit cell, and this is consistent with our Mössbauer studies. Furthermore, an analysis of the thermal parameters of the ring carbon atoms indicates that this is not the result of a disordered localized structure.

Table VIII. Comparison of the Atomic Distances (Å) of 2 and 4 with Those of 1′,1‴-Bis(*p*-bromobenzyl)biferrocene (11)

	11	2	4
Fe–C(Cp ring)	2.047 (3)	2.066 (6)	2.066 (8)
Fe–C(fulvalenide)	2.047 (3)	2.060 (7)	2.060 (8)
COM–COM[a]	3.3023 (5)	3.344 (1)	3.346 (2)
Fe–Fe	5.119 (3)	5.058 (7)	5.082 (8)
I(1)–I(2)		2.925 (2)	2.918 (1)

[a] COM is the center of mass.

As viewed down the *c* axis (Figure 3), the solid-state structure of **2** is composed of parallel sheets of mixed-valence biferrocenium cations and polyiodide ions which contain zigzag chains of alternate I_3^- and I_2 units. This unusual well-established polyiodide is not seen in the three structurally characterized biferrocenium triiodide salts.[5,13] This type of arrangement, alternating I_3^- and I_2, is quite

(20) Mammano, N. J.; Zalkin, A.; Landers, A.; Rheingold, A. L. *Inorg. Chem.* **1977**, *16*, 297.

(21) Bats, J. W.; deBoer, J. J.; Bright, D. *Inorg. Chim. Acta* **1971**, *5*, 605.

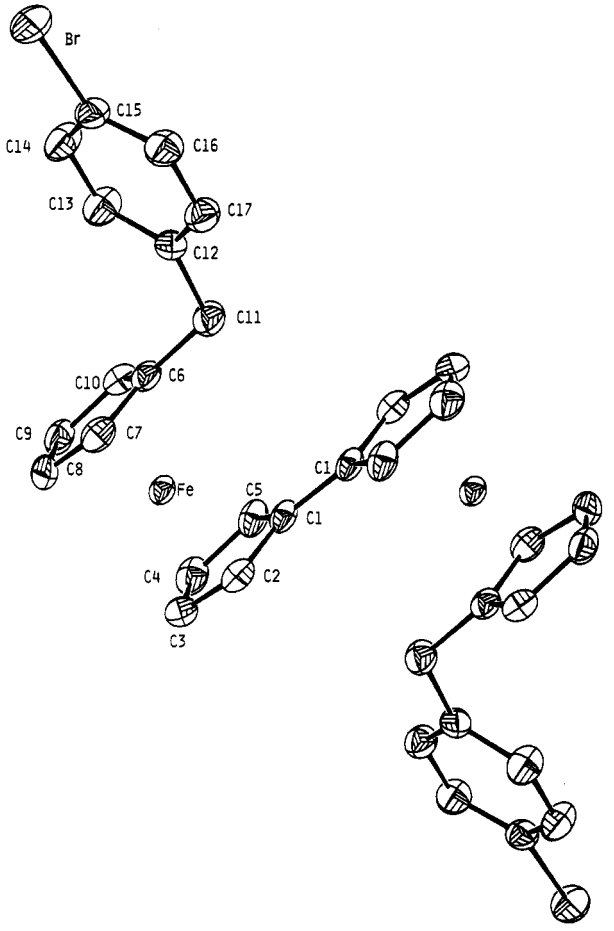

Figure 1. ORTEP plot of 1′,1‴-bis(*p*-bromobenzyl)biferrocene with 50% probability thermal ellipsoids.

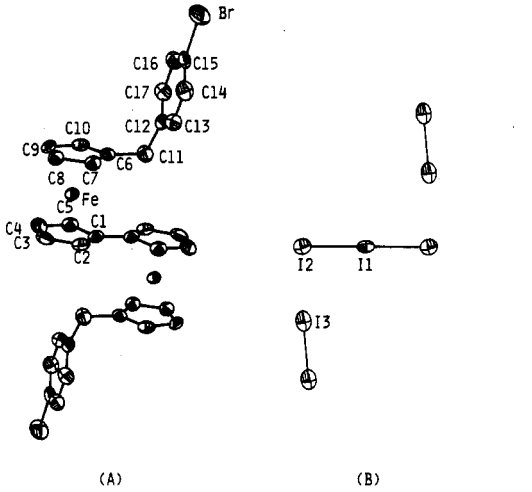

Figure 2. ORTEP plot of the 1′,1‴-bis(*p*-bromobenzyl)biferrocene cation in **2** (A) and the zigzag configuration of the polyiodide chain in **2** (B). Both are plotted with 30% probability ellipsoids.

common among the pentaiodide salts, for example, bis(phenacetin)-hydrogen iodine triiodide,[22] quinuclidinium iodine triiodide,[23] and diferrocenylselenium iodine triiodide–0.5-methylene chloride.[24] The I–I distance in the centrosymmetric I_3^- ion is 2.925 (2) Å, which is in accord with the standard value of 2.920 Å proposed for the I_3^- ion.[25] The bond length in the I_2 molecule is 2.741 (2) Å, significantly larger than the value of 2.68 Å found in crystalline I_2.[26] The distance of 3.486 (2) Å between neighboring iodine atoms in I_2 and I_3^- units within a chain indicates a significant interaction, in view of the in-plane intermolecular distance of 3.50 Å found[26] in crystalline I_2. The polyiodide structures are very similar in both (phenacetin)$_2$·HI_5[22] and the present compound. In both compounds all polyiodide chains are translationally equialent. Furthermore, the closest I—I contact (6.09 Å) between chains in compound **2** is longer than that (4.21 Å) in (phenacetin)$_2$·HI_5.[23]

The positioning of the I_3^- anion relative to the mixed-valence cation in **2** apparently is also unusual (Figure 3). The I_3^- moiety in **2** is parallel to the fulvalenide ligand, rather than perpendicular to the fulvalenide ligand as found in **6**,[5] **8**,[13] and **9**.[5] The most significant interaction (3.866 (2) Å) linking cations and anions in **2** is between the bromobenzyl bromine atoms and middle iodine atoms of I_3^- anions. The Br—I(1), Br—I(2), and Br—I(3) interactions are nonbonding and range from 3.866 to 4.441 Å.

Single-Crystal X-ray Structure of 4. Drawings of the molecular structure and packing arrangement are shown in Figures 4 and 5, respectively. A comparison was also made between **2** and **4** (see Table VIII). The plane of the benzylcyclopentadienyl ligand forms a dihedral angle of 4.7 (3)° with the fulvalenide plane, and the two cyclopentadienyl rings in each ferrocene moiety are nearly eclipsed with an average staggering angle of 2.32 (5)°. The Fe–Fe distance (5.082 (8) Å) in compound **4** is slightly greater than that (5.058 (7) Å) in compound **2**. Mean bond distances between the iron atom and the five carbons of a given ring and the COM–COM distance for a ferrocene moiety are very similar in both compounds **2** and **4**. The average C–C bond length (1.42 (1) Å) in the rings also agrees well with that in ferrocene (1.42 Å).[19]

We believe that the interactions between cations and anions could be changed by replacing the substituent in benzyl unit. As expected, the triiodide anion in **4** is situated differently. It is perpendicular to the fulvalenide ligand, not parallel to the fulvalenide ligand as found in **2** (see Figure 5). The most significant contact (3.871 (2) Å) between cation and anion in **4** is between the iodobenzyl iodine atom and terminal iodine atom of the I_3^- anion. In the case of **2**, the interaction (3.866 (2) Å) between the bromine atom in the benzyl unit and the middle iodine atom of I_3^- anion is observed.

^{57}Fe Mössbauer Characteristics. Mössbauer spectroscopy is a particularly useful technique for probing the electronic states of iron ions in mixed-valence biferrocenium salts. Ferrocenyl groups give spectra characterized by large quadrupole splitting (ΔE_Q) in the range 2.0–2.5 mm s^{-1}, while the spectra of the ferrocenium cations are characterized by small or vanishing quadrupole splitting.[27]

Variable-temperature Mössbauer spectra were run for compounds **1–5** and neutral 1′,1‴-bis(substituted benzyl)biferrocene. The various absorption peaks in each spectrum were fitted to Lorentzian lines, and the resulting fitting parameters are summarized in Table IX. The unoxidized compounds give a single doublet with ΔE_Q from 2.182 to 2.329 mm s^{-1}. This pattern of a single doublet is

(22) Herbstein, F. H.; Kapon, M. *Philos. Trans. R. Soc. London, Ser. A* **1979**, *291*, 199.
(23) Jander, J.; Pritzkow, H.; Trommsdorf, K.-U. *Z. Naturforsch. B* **1975**, *30*, 720.
(24) Kramer, J. A.; Herbstein, F. H.; Hendrickson, D. N. *Inorg. Chem.* **1980**, *102*, 2293.
(25) Runsink, J.; Swen-Walstra, S.; Migchelsen, T. *Acta Crystallogr. B* **1972**, *28*, 1331.
(26) Kitaigorodskii, A. I.; Khotsyanova, T. L.; Struchkov, Y. T. *Zh. Fiz. Khim.* **1953**, *27*, 780.
(27) Morrison, W. H.; Hendrickson, D. N. *Inorg. Chem.* **1975**, *14*, 2331.

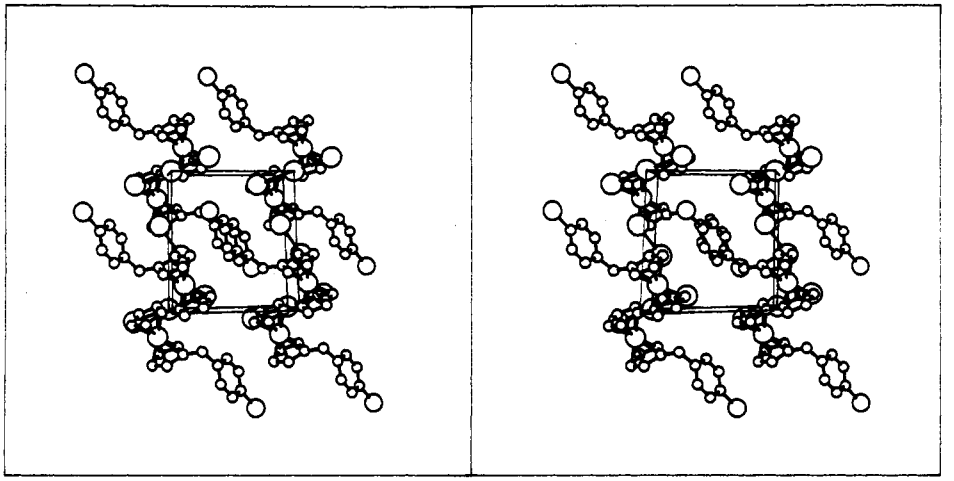

Figure 3. Stereoview of the packing arrangement of **2**, as viewed down the *c* axis.

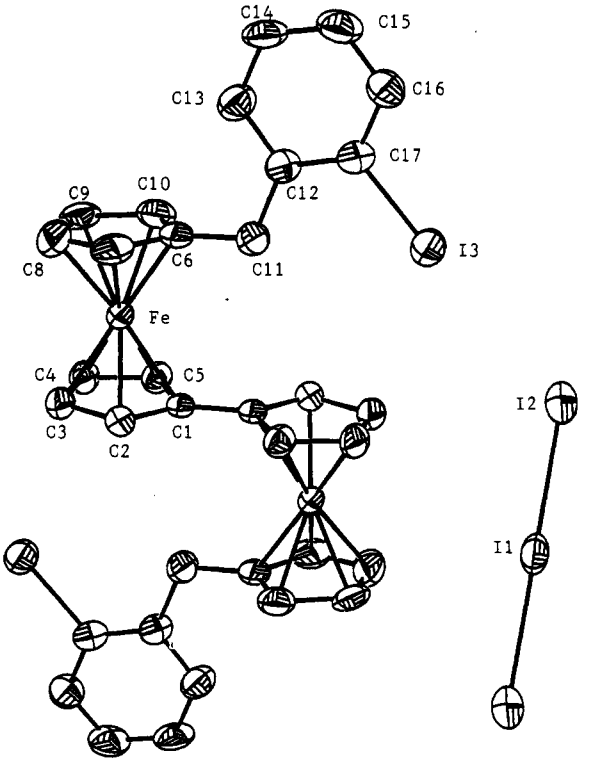

Figure 4. ORTEP plot of **4** with 30% probability thermal ellipsoids.

what is expected for a neutral biferrocene. The variable-temperature Mössbauer spectra of **1** are shown in Figure 6. The features in these spectra include two doublets which have the same area, as deduced by a least-squares fitting. This pattern of two doublets is expected for a mixed-valence biferrocenium cation which is valence trapped on the time scale of the Mössbauer technique (electron-transfer rate less than $\sim 10^7$ s^{-1}). The valence-trapped electronic structure is also seen for compound **3**. As illustrated in Figure 7, the features in the 300 K spectrum of **3** are two doublets, one with a quadrupole splitting (ΔE_Q) of 1.394 mm s^{-1} (Fe^{II} site) and the other with ΔE_Q = 0.776 mm s^{-1} (Fe^{III} site). Furthermore, both doublets have the same area by a least-squares fitting to Lorentzian line shapes. In compound **2**, at temperatures below 150 K it shows two doublets in the ^{57}Fe Mössbauer spectra. It indicates that compound **2** is valence trapped on the Mössbauer time scale (electron-transfer rate is less than $\sim 10^7$ s^{-1}) below 150 K. As shown in Figure 8, increasing the temperature for a sample of **2** causes two doublets to become a single "average-valence" doublet at temperature $\sim$200 K. In other words, the electron-transfer rate in **2** is greater than $\sim 10^7$ s^{-1} above 200 K.

There is a dramatic change in electron-transfer rate as the position of the halide substituent in the benzyl unit is changed from the para position to the ortho position. In comparison with compounds **1–3**, surprisedly, a single "average-valence" doublet ($\Delta E_Q \simeq 1.1$ mm s^{-1}) is seen at 77 K for **4** and **5** (see Figure 9). The Mössbauer data clearly indicate that the intramolecular electron-transfer rates in **4** and **5** are greater than $\sim 10^7$ s^{-1} even at 77 K. Compounds **4** and **5** have the lowest valence-detrapped transition temperature among the dialkyl analogues. Very recent, Hendrickson found that 1′,1‴-dibenzylbiferrocenium hexafluorophosphate is converted from a valence-trapped state to a valence-detrapped state at 170

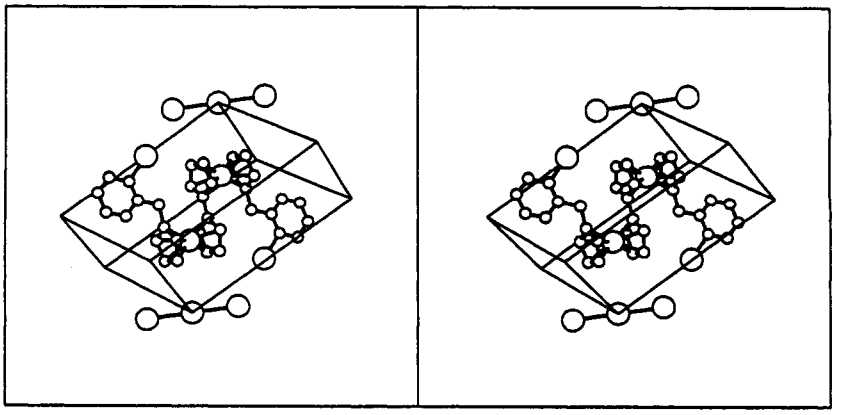

Figure 5. Stereoview of the packing arrangement of **4**.

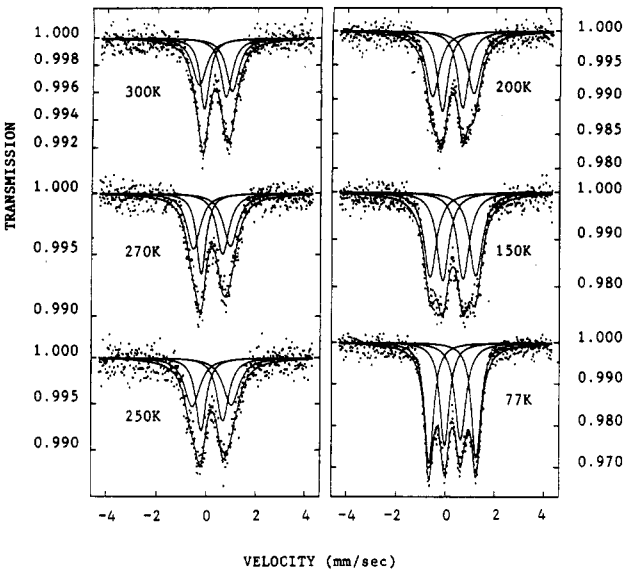

Figure 6. Variable-temperature ^{57}Fe Mössbauer spectra of 1.

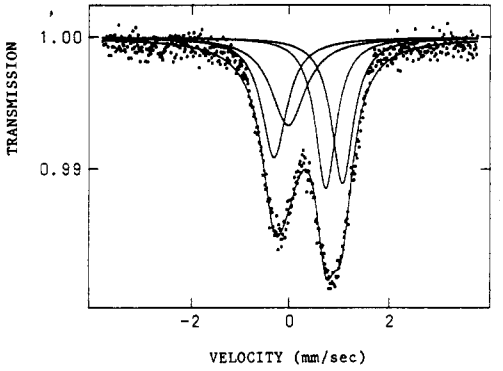

Figure 7. ^{57}Fe Mössbauer spectrum of 3.

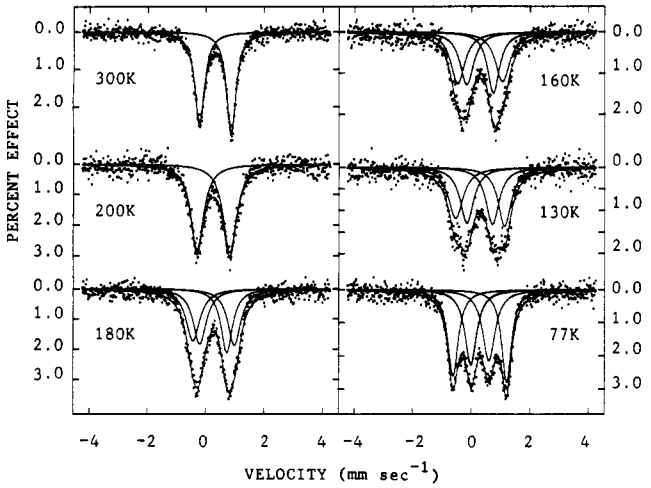

Figure 8. Variable-temperature ^{57}Fe Mössbauer spectra of 2.

K.[28] In our case, in changing from the para substitution to ortho substitution for the 1′,1‴-bis(substituted benzyl)biferrocenium cation there is a change from 300 to below 77 K for the valence-detrapped transition temperature. This difference does not originate in a difference in electronic or vibronic coupling in the cations. Evidence in support of the above statement can be gleaned from the electrochemical data for the five neutral biferrocenes. Each

(28) Webb, R. J.; Geib, S. J.; Staley, D. L.; Rheingold, A. L.; Hendrickson, D. N. *J. Am. Chem. Soc.* **1990**, *112*, 5031.

Table IX. ^{57}Fe Mössbauer Least-Squares-Fitting Parameters for Neutral and Mixed-Valence Biferrocenes

compd[a]	T, K	ΔE_Q, mm/s	δ,[b] mm/s	Γ,[c] mm/s
1′,1‴-bis(*p*-iodobenzyl)bifc	300	2.308	0.437	0.315, 0.322
1′,1‴-bis(*p*-bromobenzyl)bifc	300	2.309	0.440	0.281, 0.292
1′,1‴-bis(*p*-chlorobenzyl)bifc	300	2.297	0.437	0.301, 0.318
1′,1‴-bis(*o*-iodobenzyl)bifc	300	2.329	0.443	0.228, 0.281
1′,1‴-bis(*o*-bromobenzyl)bifc	300	2.319	0.439	0.261, 0.266
1	300	1.351	0.417	0.620, 0.702
		0.890	0.406	0.559, 0.466
	270	1.513	0.309	0.695, 0.663
		0.886	0.318	0.605, 0.457
	250	1.589	0.321	0.775, 0.751
		0.899	0.340	0.581, 0.503
	200	1.685	0.367	0.672, 0.643
		0.833	0.346	0.548, 0.524
	150	1.858	0.392	0.621, 0.614
		0.835	0.399	0.600, 0.588
	77	1.940	0.402	0.448, 0.443
		0.661	0.406	0.538, 0.468
2	300	1.096	0.430	0.385, 0.405
	200	1.130	0.372	0.554, 0.531
	180	1.417	0.395	0.538, 0.583
		0.924	0.366	0.478, 0.552
	160	1.517	0.403	0.603, 0.579
		0.906	0.411	0.488, 0.566
	130	1.677	0.409	0.527, 0.609
		0.884	0.401	0.544, 0.556
	77	1.840	0.405	0.399, 0.428
		0.620	0.414	0.519, 0.488
3	300	1.394	0.491	0.522, 0.635
		0.776	0.474	0.505, 0.864
4	300	1.179	0.432	0.336, 0.293
	77	1.242	0.406	0.383, 0.379
5	300	1.136	0.429	0.321, 0.307
	77	1.175	0.402	0.427, 0.426

[a] bifc is biferrocene. [b] Isomer shifts. [c] Full width at half-height taken from the least-squares-fitting program. The width for the line at more positive velocity is listed first for each doublet.

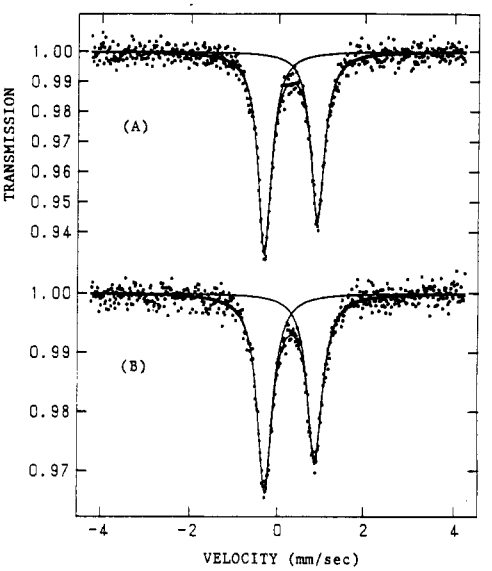

Figure 9. ^{57}Fe Mössbauer spectra of 4 (A) and 5 (B) at 77 K.

shows two one-electron oxidation waves ($E_{1/2}$ = 0.32 and 0.64 V), and the separation (0.32 V) between the two one-electron oxidation waves is the same. The difference of electron-transfer rates can be explained by the difference of packing arrangements for triiodide anions. More detailed discussion will be presented in the last section.

Electron Paramagnetic Resonance. With the ^{57}Fe Mössbauer data of 4 and 5 in hand, it is necessary to determine whether the electron-transfer rates in 4 and 5 are greater than the EPR time scale or not. The X-band EPR spectra were run at 77 K for samples of 1–5. An axial-type spectrum was observed for the series of compounds. The g values extracted from all of these spectra are collected in Table X, together with some g values from

Table X. Electron Paramagnetic Resonance Data[a]

compd	T, K	$g_\parallel$	$g_\perp$	Δg^b
ferrocenium triiodide[c]	20	4.35	1.26	3.09
6[d]	4.2	3.66	1.73	1.93
7[d]	4.2	3.02	2.01; 1.89	1.07
9[d]	4.2	2.98	1.92	1.06
1	77	3.23	1.94	1.29
2	77	3.14	1.91	1.23
3	77	3.35	1.86	1.49
4	77	2.97	1.95	1.02
5	77	3.10	1.93	1.17

[a] Powder samples. [b] This is the g-tensor anisotropy defined as $\Delta g = g_\parallel - g_\perp$. [c] See refs 30 and 31. [d] See ref 32.

Table XI. IR Data (cm^{-1}) for the C–H Bending Mode

	C–H bending mode	
compd[a]	Fe(II)	Fe(III)
1′,1‴-bis(*p*-iodobenzyl)bifc	809	
1	817	834
1′,1‴-bis(*p*-bromobenzyl)bifc	810	
2	818	832
1′,1‴-bis(*p*-chlorobenzyl)bifc	810	
3	816	840
1′,1‴-bis(*o*-iodobenzyl)bifc	810	
4	820	835
1′,1‴-bis(*o*-bromobenzyl)bifc	812	
5	818	834

[a] bifc is biferrocene.

the literature. From Table X, it can be seen that ferrocenium triiodide[29-31] gives an axial EPR signal. The g-tensor anisotropy, $\Delta g = g_\parallel - g_\perp$, is 3.09 for ferrocenium triiodide. The influence of substituents on the EPR signal has been studied for a number of ferrocenium complexes.[31] In the case of binuclear mixed-valence biferrocenium ions, a reduction of Δg was seen.[32] It has been suggested[32] that Δg can be used to determine whether the rate of electron transfer is greater than the EPR time scale or not. If $\Delta g < 0.8$, then the rate of intramolecular electron transfer in biferrocenium cation is greater than the EPR time scale (10^9–10^{10} s^{-1}). From Table X, the Δg values for **1–5** suggest that the cations in these compounds are localized on the EPR time scale at 77 K.

IR Spectroscopy. IR spectroscopy has proven to be useful to tell whether a given mixed-valence biferrocenium cation is delocalized or not.[5,33] When iron(II) metallocene is oxidized to iron(III) metallocene, there is a dramatic change in the IR spectrum. It has been shown[33] that the perpendicular C–H bending band is the best diagnosis of the oxidation state. This band is seen at 815 cm^{-1} for ferrocene and at 851 cm^{-1} for ferrocenium triiodide. Mixed-valence biferrocenium cations that have a nonnegligible potential energy barrier for electron transfer should exhibit one C–H bending band for the Fe^{II} moiety and one for the Fe^{III} moiety.

Infrared spectra were run for KBr pellets of **1–5** and unoxidized biferrocenes. In the perpendicular C–H bending region there is a strong band at ~810 cm^{-1} for each of unoxidized biferrocenes (see Table XI). The mixed-valence compounds **1–5** show relatively strong bands at ~816 and 835 cm^{-1}. It is clear that, on the IR time scale, the mixed-valence cations **1–5** have both Fe^{II} and Fe^{III} moieties. In other words, the electron-transfer rates in the series of **1–5** are less than ~10^{12} s^{-1} at 300 K.

Valence Detrapping in 2 and 4. The goal of this section is to present an explanation for the pronounced influence that the substituents have on the rates of intramolecular electron transfer in mixed-valence biferrocenium salts **2** and **4**.

In Hendrickson's theoretical model,[12] the factors that are potentially important in controlling the rate of intramolecular electron transfer in a mixed-valence biferrocenium cation include (1) the effective barrier for electron transfer in the cation, (2) the effective barrier for charge oscillation in the anion, and (3) the intermolecular cation–cation and cation–anion interactions. In general, it has been suggested that the greater the effective barrier for charge oscillation in the cation or anion, the smaller the electron-transfer rate.

In our previous papers,[5,9,10] it has been found that the nature of the solid-state environment about a mixed-valence biferrocenium cation can have a dramatic impact on the rate of intramolecular electron transfer. We suggested that it is the onset of vibrational motion involving the I_3^- counterion that controls the rate of intramolecular electron transfer in the mixed-valence biferrocenium triiodide salts. When the I_3^- counterion is thermally activated, it interconverts between two configurations, $I_a^-\cdots I_b-I_c$ and $I_a-I_b\cdots I_c^-$. In each of these limiting forms the two iodine–iodine bond lengths are not equal. In fact, the I_3^- counterion is a mixed-valence species and the oscillatory charge motion associated with it controls whether charge can be pulled back and forth in the mixed-valence cation. The thermal barrier for I_3^- interconverting between these two configurations has been estimated to be ~250 cm^{-1}.[34]

It is our suggestion that the dramatic difference in electron-transfer rates between **2** and **4** results from the difference of packing arrangements for triiodide anions. As discussed in the X-ray sections, the triiodide anion in **4** is perpendicular to the fulvalenide ligand, not parallel to the fulvalenide ligand as found in **2**. In other words, the charge oscillation of I_3^- anion in **4** is parallel to the electron-transfer pathway and this leads to a decrease in the thermal energy barrier of charge oscillation in the cation of **4**. In the solution state, the charge oscillation barrier for a mixed-valence biferrocenium cation has been estimated to be ~1200 cm^{-1}.[27] However, in the solid state, the rate of electron transfer for a mixed-valence cation is influenced by various structural factors and lattice dynamics, including the nature of the charge motion in the counterion and cation–anion interaction. For a mixed-valence biferrocenium triiodide, the I_3^- anion has to be disposed symmetrically relative to both iron ions and has to move rapidly so that it does not limit the rate of intramolecular electron transfer. Thus, the position of the I_3^- anion can have a pronounced influence on the rate of electron transfer. The cation gains more delocalization energy when the two charge oscillations in the cation and anion are parallel.

Concluding Comments

In this paper, we demonstrate that relatively minor perturbations caused by interactions with neighboring cations and anions in biferrocenium salts experiencing weak or moderate electronic coupling between two Fe centers have pronounced effects on the electronic structure and rate of intramolecular electron transfer. It seems likely

(29) Anderson, S. E.; Rai, R. *Chem. Phys.* **1973**, *2*, 216.
(30) Sahn, Y. S.; Hendrickson, D. N.; Gray, H. B. *J. Am. Chem. Soc.* **1971**, *93*, 3603.
(31) Duggan, D. M.; Hendrickson, D. N. *Inorg. Chem.* **1975**, *14*, 955.
(32) Dong, T.-Y.; Hendrickson, D. N.; Pierpont, C. G.; Moore, M. F. *J. Am. Chem. Soc.* **1986**, *108*, 963.
(33) Kramer, J. A.; Hendrickson, D. N. *Inorg. Chem.* **1980**, *19*, 330.
(34) Brown, R. D.; Nunn, E. K. *Aust. J. Chem.* **1966**, *19*, 1567.

that the position of the I_3^- anion caused a dramatic influence on the rates of electron transfer in **2** and **4**.

Recently, the influence of solvate molecule motion on the properties of mixed-valence iron acetate complexes has been recognized.[35] A phase transition involving the onset of solvate dynamics was found in these iron acetate complexes. Furthermore, the phase transitions were established with heat capacity measurements. It would be very instructive if one could employ thermal analysis on mixed-valence complexes **1-5** to determine whether the I_3^- anions are or are not rapidly oscillating between two vibronic states.

(35) Jang, H. G.; Geib, S. J.; Kaneko, Y.; Nakano, M.; Sorai, M.; Rheingold, A. L.; Montez, B.; Hendrickson, D. N. *J. Am. Chem. Soc.* **1989**, *111*, 173.

Acknowledgment. We are grateful for support from the National Science Council.

Registry No. **1**, 135568-59-1; **2**, 138208-46-5; **3**, 125840-44-0; **4**, 135568-52-4; **5**, 135568-55-7; **11**, 135568-53-5; 1′,1‴-bis(*p*-chlorobenzyl)biferrocene, 138208-47-6; 1′,1‴-bis(*p*-iodobenzyl)-biferrocene, 138208-48-7; 1′,1‴-bis(*o*-bromobenzyl)biferrocene, 138208-49-8; 1′,1‴-bis(*o*-iodobenzyl)biferrocene, 138208-50-1; 1′,1‴-bis(*p*-bromobenzoyl)biferrocene, 138208-51-2; 1′,1‴-bis(*p*-iodobenzoyl)biferrocene, 138208-52-3; 1′,1‴-bis(*o*-bromobenzoyl)biferrocene, 138208-53-4; 1′,1‴-bis(*o*-iodobenzoyl)biferrocene, 138208-54-5.

Supplementary Material Available: Tables of thermal parameters for 1′,1‴-bis(*p*-bromobenzyl)biferrocene, **2**, and **4** (4 pages); tables of structure factors for the same three compounds (52 pages). Ordering information is given on any current masthead page.

Kinetics and Mechanism of the Outer-Sphere Oxidation of Metal Carbonyl Anions with Coordination Complexes Containing Chloride

C. K. Lai, M. Shauna Corraine, and Jim D. Atwood*

Department of Chemistry, University at Buffalo, State University of New York, Buffalo, New York 14214

Received June 24, 1991

Reactions of metal carbonyl anions, $CpFe(CO)_2^-$, $Re(CO)_5^-$, $Mn(CO)_5^-$, $CpMo(CO)_3^-$, $CpCr(CO)_3^-$, and $Co(CO)_4^-$, with $CrCl_3 \cdot 3S$ (S = THF, CH_3CN) and reactions of $Mn(CO)_5^-$ and $Re(CO)_5^-$ with $[Co(o\text{-phen})_2Cl_2]ClO_4$ are reported. Net oxidation/reduction chemistry is observed with formation of metal carbonyl dimers and $CrCl_2 \cdot 4S$ or $Co(o\text{-phen})_2Cl_2$. Metal carbonyl halides are also observed and shown to arise from a secondary reaction of the metal carbonyl dimer with the oxidant. The products and rates are most consistent with outer-sphere electron-transfer reactions. Reactions of $CpFe(CO)_2^-$ with $CpFe(CO)_2X$ (X = Cl, Br, I) are also reported. The rate dependence on X is very small and in the order expected for nucleophilic substitution.

The close relationship between S_N2 and SET (single-electron-transfer) mechanisms in reactions of organic anions with halide-containing compounds continues to be explored.[1] The inorganic analogues of inner-sphere and outer-sphere electron transfer have remained distinct due to the requirement of a coordination site for an inner-sphere process.[2] However, reactions of the metal carbonyl anions are not as easy to classify into mechanisms. Reactions with MeI have been used to define the nucleophilicity for the metal carbonyl anions.[3] Evaluation of the oxidation potentials and reactions with outer-sphere electron acceptors has been used to establish the outer-sphere reactivity of the metal carbonyl anions.[4] Unfortunately, as might be expected, the order of the metal carbonyl anions in nucleophilic reactions[3]

$$CpFe(CO)_2^- > Re(CO)_5^- > Mn(CO)_5^- > CpMo(CO)_3^- > Co(CO)_4^-$$

is the same as for outer-sphere reactions.[4c] From the data collected thus far the change in rate with nucleophilicity is larger (10^8 for the anions listed)[3] in comparison to reaction with outer-sphere acceptors (10^4 for the anions listed).[4c] The similarity in order makes it very difficult to distinguish between an outer-sphere (or SET) mechanism and an inner-sphere electron-transfer mechanism that is initiated by nucleophilic attack by the anion.

$$2M^- + 2oxidant \rightarrow [2M^\bullet + 2oxidant^-] \rightarrow M_2 + 2oxidant^- \quad (1)$$

$$2M^- + 2oxidant \rightarrow 2[M\text{–}oxidant] \rightarrow [2M^\bullet + 2oxidant^-] \rightarrow M_2 + 2oxidant^- \quad (2)$$

The two mechanisms differ only in the presence of the nucleophile–electrophile adduct in the inner-sphere mechanism. The difficulty in distinguishing between these two is more related to the SET and S_N2 mechanisms in organic reactions than differentiation between inorganic electron-transfer mechanisms.[1]

Reactions of metal carbonyl anions with metal carbonyl halides have been used to form metal–metal bonds, es-

(1) (a) Shaik, S. S. *Acta Chem. Scand.* **1990**, *44*, 205 and references therein. (b) Newcomb, M.; Curran, D. P. *Acc. Chem. Res.* **1988**, *21*, 206 and references therein. (c) Ashby, E. C. *Acc. Chem. Res.* **1988**, *21*, 414 and references therein.

(2) (a) Atwood, J. D. *Inorganic and Organometallic Reaction Mechanisms*; Brooks/Cole: Monterey, CA, 1985. (b) Wilkins, R. G. *The Study of Kinetics and Mechanisms of Reactions of Transition Metal Complexes*; Allyn and Bacon: New York, 1974. (c) Basolo, F.; Pearson, R. G. *Mechanisms of Inorganic Reactions*; Wiley: New York, 1968.

(3) (a) Lai, C. K.; Feighery, W. G.; Zhen, Y.; Atwood, J. D. *Inorg. Chem.* **1989**, *28*, 3929. (b) Pearson, R. G.; Figdore, P. E. *J. Am. Chem. Soc.* **1980**, *102*, 1541. (c) Dessy, R. E.; Pohl, R. L.; King, R. B. *J. Am. Chem. Soc.* **1966**, *88*, 5121.

(4) (a) Tilset, M.; Parker, V. D. *J. Am. Chem. Soc.* **1989**, *111*, 6711. (b) Corraine, M. S.; Atwood, J. D. *Organometallics* **1991**, *10*, 2315. (c) Lai, C. K.; Corraine, M. S.; Zhen, Y.; Churchill, M. R.; Buttrey, L. A.; Ziller, J. W.; Atwood, J. D. *Organometallics*, in press.

0276-7333/92/2311-0582$03.00/0